JACS
JOURNAL OF THE AMERICAN CHEMICAL SOCIETY
Communication
pubs.acs.org/JACS

An $FeF_3 \cdot 0.5H_2O$ Polytype: A Microporous Framework Compound with Intersecting Tunnels for Li and Na Batteries

Chilin Li,*[,†,‡] Congling Yin,[‡] Lin Gu,[§] Robert E. Dinnebier,[‡] Xiaoke Mu,[∥] Peter A. van Aken,[∥] and Joachim Maier[‡]

[†]State Key Laboratory of High Performance Ceramics and Superfine Microstructure, Shanghai Institute of Ceramics, Chinese Academy of Sciences, Shanghai 200050, China

[‡]Max Planck Institute for Solid State Research, Heisenbergstraße 1, D-70569 Stuttgart, Germany

[§]Beijing National Laboratory for Condensed Matter Physics, Institute of Physics, Chinese Academy of Sciences, Beijing 100190, China

[∥]Max Planck Institute for Intelligent Systems, Heisenbergstraße 3, D-70569 Stuttgart, Germany

Supporting Information

ABSTRACT: To improve the energy/power density of energy storage materials, numerous efforts have focused on the exploration of new structure prototypes, in particular metal−organic fameworks, Prussian blue analogues, open-framework oxides, and polyanion salts. Here we report a novel pyrochlore phase that appears to be useful as a high-capacity cathode for Li and Na batteries. It is an iron fluoride polymorph characterized by an intersecting tunnel structure, providing the space for accommodation and transport of Li and Na ions. It is prepared using hydrolyzable ionic liquids, which serve as reaction educts and structure-directing agents not only as far as the chemical structure is concerned but also in terms of morphology (shape, defect structure, electrode network structure). A capacity higher than 220 mA h g^{-1} (for Li and Na storage) and a lifetime of at least 300 cycles (for Li storage) are demonstrated.

Recently, low-density porous framework solids, such as materials based on metal−organic frameworks (MOFs), zeolitic frameworks, or Prussian blue (PB) analogues, have been attracting significant attention because of their diverse applications as energy storage materials, proton conductors, wide-band-gap semiconductors, catalysts, selective gas absorbers, and nanoporous carbon precursors.[1] These phases are generally assembled at low temperature by precipitation, solvothermal, or ionothermal synthesis. Ionic liquids (ILs) are well-suited candidates as reaction media, with the cations potentially serving as structure-directing templates to order and polymerize surrounding inorganic/organic units, likely leading to structural expansion with lowered crystal density.[1e] This strategy was recently discovered to be especially useful for developing novel open-structure Li storage cathodes (e.g., tavorite polyanion frameworks or iron fluoride polymorphs[2,3]) that are characterized by enhanced ion transport in multidimensional channels and extended solid-solution reaction zones.

Electroactive MOFs and PB analogues exhibit quite open channels, the sizes of which may even reach the mesoporous range and hence exceed the optimal width for ion insertion. Furthermore, these frameworks are usually of high molecular weight because of their heavy skeletons and/or the existence of channel fillers. As far as electrochemical storage is concerned, these factors limit the reversible capacity as reported by Férey et al.[1a] and Okubo et al.[1b] in the context of Li batteries (usually <100 mA h g^{-1}). In terms of electrochemical storage, not only are Li-based batteries of interest, but also in view of globally limited Li resources, Na-based batteries are seen as a potential alternative for both electric vehicles and large-scale grid-based electrical energy storage.[4] As the ionic radius of Na^+ (1.02 Å) is 34% larger than that of Li^+ (0.76 Å),[5] suitable Li storage materials are not automatically feasible for Na batteries, and in turn, channels that are oversized for Li may be well-suited for Na, as recently reported for several PB analogues.[1b,6]

To further improve the energy/power density of Li- or Na-based batteries, structure modification of oxide/polyanion materials with moderate expansion of ion channels has been demonstrated to be a successful strategy.[7,8] In most cases, the reversible Li and even Na storage capacity can exceed 100 mA h g^{-1}, which is higher than that of MOF and PB analogues. However, one should pay attention to the fact that the synthesis of more expanded structures usually comes at the cost of a decrease in ion channel dimensionality, mostly leading to the formation of 1D or 2D channel structures that have a greater potential to become blocked or degraded.[7,8a] Also, in the case of interconnected open 3D channels, structure expansion upon storage is still a great challenge. Fluorides are expected to exhibit larger capacities than most of the oxides without tradeoffs in terms of working voltage as long as their poor conductivity can be compensated.[9] In the past decades, such studies mainly focused on commercially available ReO_3-type FeF_3 electroactivated by high-energy ball milling of FeF_3/C composites to generate C−FeF_3 nanodomains as 3 V composite cathodes for Li batteries.[9a,b] Okada and co-workers attempted to apply this material in Na batteries.[10] However, the performance deteriorated seriously compared with Li batteries, likely because of the dense structure of FeF_3. Most recently, our group prepared an open-structure fluoride for Li battery applications.[3] As reported for the

Received: March 1, 2013
Published: July 18, 2013

   dx.doi.org/10.1021/ja402061q | J. Am. Chem. Soc. 2013, 135, 11425−11428

hexagonal tungsten−bronze (HTB)-type compound $FeF_3{\cdot}0.33H_2O$ characterized by open 1D channels, the Li insertion mechanism was intrinsically modified, and the miscibility gap present in ReO_3-type FeF_3 was completely removed in the HTB phase, favoring complete solid-solution behavior in the 3 V region.[3b] An improved intrinsic conductivity enabled the fluoride to act as a highly electroactive Li battery cathode without in situ addition of conductive species. However, the presence of single ion channels, which are prone to partial blockage by H_2O molecule fillers, still limits the extension of fluoride materials into Na batteries.

Here we report a novel open-framework fluoride pyrochlore phase, $FeF_3{\cdot}0.5H_2O$, that is structurally similar to the known $AlF_3{\cdot}0.5H_2O$[11] and characterized by a much larger cell volume (∼1130 Å^3) than in HTB-type $FeF_3{\cdot}0.33H_2O$ (∼710 Å^3) or ReO_3-type FeF_3 (∼310 Å^3).[3b,9b] Notably, it exhibits a higher pore density due to interconnected 3D ion channels without a serious tradeoff concerning channel size compared with HTB-type fluoride, suggesting a more favorable cation insertion capacity (especially for the larger Na^+ to achieve a high capacity of >200 mA h g^{-1}). The storage performance should also benefit from the more tightly confined H_2O molecules in the zigzag channels of the pyrochlore phase as opposed to the straight channels of the HTB phase. In a typical IL-based precipitation method, IL cations of different size can significantly influence the crystallinity, cavity size, and surface defect concentration of the pyrochlore phase. In the following, we discuss the IL-dependent fluoride nucleation/growth process and the remarkable effects of the IL on the carbon nanotube wiring and Li/Na storage performance.

Two hydrophilic BF_4^--based ILs with cations having different alkyl chain lengths, 1-butyl-3-methylimidazolium tetrafluoroborate ($BmimBF_4$) and 1-decyl-3-methylimidazolium tetrafluoroborate ($C_{10}mimBF_4$), were selected as reaction media for the precipitation of the pyrochlore polymorph of $FeF_3{\cdot}0.5H_2O$. Powder X-ray diffraction (PXRD) confirmed its formation and showed the absence of impurity phases. The PXRD patterns [Figure 1a and Figure S1a in the Supporting Information (SI)] were well-fitted by Rietveld refinement according to the $AlF_3{\cdot}0.5H_2O$ structure model (R_{wp} = 9.4−10.5%).[11] In this typical pyrochlore structure, (Figure 1b and Table S1 in the SI), Fe atoms are sixfold-coordinated by F atoms, while F atoms are twofold-coordinated by Fe atoms. Six FeF_6 octahedra are connected one by one by sharing of vertex F atoms, leading to the formation of hexagonal cavities, which are building elements of an interconnected 3D microporous framework with quite a large cell volume (1127−1131 Å^3). To provide a clear view of the pores' connectivity, in Figure 1c only the central Fe atoms of the FeF_6 octahedra and the trapped O atom are shown. Four close-packed $(FeF_6)_4$ tetramers are connected to each other by vertices to form a $(FeF_6)_{16}$ supertetrahedron that contains a truncated tetrahedral cavity with the dimension $\Phi_c = 2[D_{CF} - r_w(F)]$, where D_{CF} denotes the distance between the cavity center and the nearest F atom and $r_w(F)$ is the van der Waals radius of F atom. In this 3D network, the cavities connect with each other by sharing hexagonal faces [dimension $\Phi_h = D_{FF} - 2r_w(F)$, where D_{FF} is the distance between the diagonal fluorine atoms in a hexagon of FeF_6 octahedra]. The cavities, with diameters of 3.38 Å for $BmimBF_4$ and 3.52 Å for $C_{10}mimBF_4$, are large enough to accommodate one H_2O molecule. The hexagonal faces, which are 2.29 and 2.39 Å in diameter for $BmimBF_4$ and $C_{10}mimBF_4$, respectively, act as ion-exchange pathways between the cavities. The slightly larger size of the characteristic cavity as defined

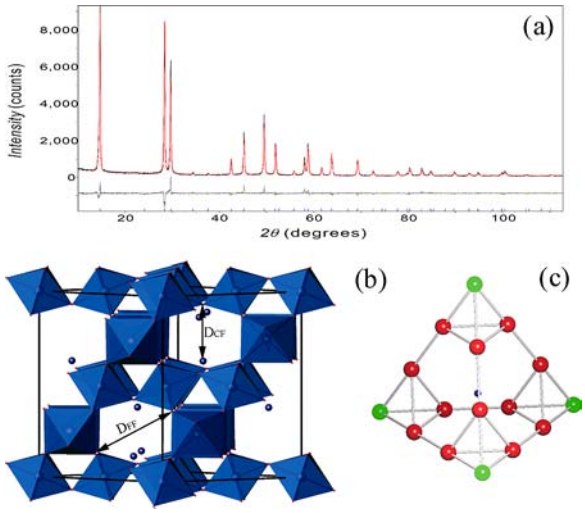

Figure 1. (a) PXRD pattern and its Rietveld refinement for pyrochlore-type $FeF_3{\cdot}0.5H_2O$ wired with 5 wt % SWNTs precipitated from $C_{10}mimBF_4$. (b) Structure of pyrochlore-type $FeF_3{\cdot}0.5H_2O$ with a cubic lattice. FeF_6 octahedra and tunnel O atoms are shown in blue. D_{CF} is the distance between the cavity center and the nearest F atom. D_{FF} is the distance between the diagonal F atoms in a hexagon of FeF_6 octahedra. (c) Simplified sketch of a $(FeF_6)_{16}$ supertetrahedron with its truncated tetrahedral cavity. The central Fe atoms of the FeF_6 octahedra are shown in red and green, and the trapped O atom is shown in blue.

above arises from the action of the larger $C_{10}mim^+$ moiety as a structure-directing agent. The good thermal stability of the pyrochlore phase and the presence of waters of hydration were confirmed by thermogravimetric analysis coupled with mass spectroscopy (TGA−MS) as well as PXRD patterns after annealing at different temperatures (Figure S2).

The microscopic morphology of the network formed by fluoride particles and wired by single-walled carbon nanotubes (SWNTs) strongly depended on the imidazolium cation of the IL, which can disentangle SWNT clusters via interactions with the π electrons at the SWNT surface.[3c,12] When $BmimBF_4$ was used, irregular submicrometric grains of fluoride composites tended to assemble into much larger micrometer-sized aggregates with few large voids or cracks [see the scanning electron microscopy (SEM) images in Figures 2d and S3a). The surface of the aggregates was relatively homogeneous, and grain boundaries could not easily be discerned. Unexpectedly, only a few SWNTs could be observed wrapping around the grain surface; most of them were fragmentated and confined in the grain interior [see the transmission electron microscopy (TEM) images in Figure 2e,f]. Actually, the composite grains were composed of numerous spherical fluoride nanoparticles (NPs) as small as ∼10 nm embedded in a fragmented or amorphized SWNT matrix. Furthermore, in the annular bright-field scanning TEM (ABF-STEM) image in Figure 2i, few-layer nanographene encapsulation (<7 stacked monolayers, ∼2 nm) could be observed on almost every NP surface (see Figure S4 for more examples). In contrast, $C_{10}mimBF_4$ significantly promoted the separation of grains with evidently discernible grain boundaries, most of which were regular octahedron-shaped crystals (growing along the [111] direction of the cubic lattice) with sizes of 200−300 nm (Figures 2a−c and S3b), in agreement with the much more intense diffraction peaks (Figure S1b). The SWNTs did not appear to uniformly wire the grains but rather were locally entangled at the regions where a lot of much smaller NPs

dx.doi.org/10.1021/ja402061q | J. Am. Chem. Soc. 2013, 135, 11425−11428

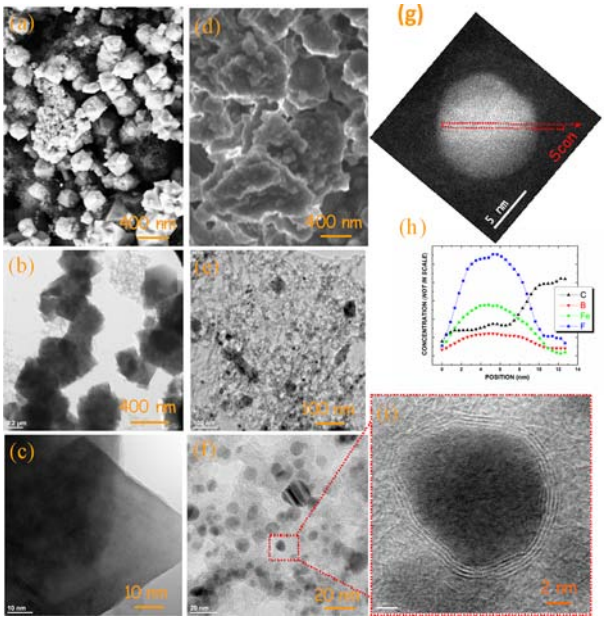

Figure 2. (a, d) SEM images of SWNT (5 wt %)-wired $FeF_3{\cdot}0.5H_2O$ precipitated from (a) $C_{10}mimBF_4$ and (d) $BmimBF_4$. (b) TEM and (c) HRTEM images of wired $FeF_3{\cdot}0.5H_2O$ from $C_{10}mimBF_4$, mainly consisting of octahedron-shaped crystal grains (200−300 nm). (e, f) TEM images of wired $FeF_3{\cdot}0.5H_2O$ from $BmimBF_4$, characterized by spherical NPs (∼10 nm) embedded in a fragmentated SWNT matrix. (g) HAADF-STEM image of a single NP. (h) Elemental line profiles of C, B, Fe, and F recorded along the red arrow in (g). (i) ABF-STEM image of a microporous NP encapsulated by few-layer nanographene.

assembled. These NPs were naturally more attractive toward SWNTs as opposed to neighboring larger crystal grains.[3c]

To acquire deeper insight into the formation mechanism of graphitic encapsulation in the $BmimBF_4$-based synthesis, exploration of a single fluoride NP was necessary. Electron energy-loss spectroscopy (EELS) and high-angle annular-dark-field STEM (HAADF-STEM) revealed the corresponding elemental profiles of C, B, F, and Fe (Figure 2g,h) using the C K, B K, F K, and Fe L edges, respectively. One finding is that the spatial distribution of B was similar to that of Fe and F, indicating that there is sufficient IL component (at least from the anion) entrapped at the particle surface. In contrast, the C concentration increased outside the NP, verifying that NPs were embedded in the graphene-like layers as stated before. Apart from $BmimBF_4$ anion trapping, the $Bmim^+$ cation could also be adsorbed on the surface of pyrochlore NPs as demonstrated by X-ray photoelectron spectroscopy (XPS) (Figure S5).

Ex-situ PXRD patterns for various stages of electrochemical lithiation indicated that lithiation irreversibly amorphized the pyrochlore framework (Figure S6). Combined with our recent discovery that amorphization is also caused by the removal of hydration water,[13] one can conclude that guest stuffing is another important factor in disordering or amorphizing pyrochlore phases apart from ion irradiation, pressure, and temperature.[14] However, the short-range order was still likely preserved during the facile amorphization, as indicated by the following voltage versus capacity profiles. The denser HTB-type $FeF_3{\cdot}0.33H_2O$ was shown to be structurally more stable during lithiation/delithiation.[3b] However, it cannot be used as a backup for graphitic encapsulation.[3c] LiF nanodomains were formed during lithiation, as observed from the emergence of broad LiF diffraction peaks, which were not observed from the $FeF_3{\cdot}0.33H_2O$ samples.[3b] The formation/decomposition of LiF was not electrochemically reversible, as its diffraction peaks were still present after charging. The appearance of LiF was unexpected. We speculate that it is likely associated with the reaction of surface defects rather than the conversion reaction, which actually does not occur at such high working voltages. The LiF peaks were much weaker for the samples prepared from $C_{10}mimBF_4$ than from $BmimBF_4$ at corresponding lithiation depths (Figure S6b), possibly suggesting fewer surface defects due to crystal growth of the pyrochlore phase. The defect enrichment at the NP surface was further indicated by the blurred lattice stripes and lighter contrast close to the particle edges in the ABF-STEM images (Figure S4).

As known, the added SWNTs are uniformly capped by IL, with the cations oriented toward the SWNT surface.[3c] After the addition of the Fe(III) precursor, fast nucleation occurs around the outward-stretched BF_4^- moieties, which can be hydrolyzed into F^- ion and $BF_3{\cdot}H_2O$.[15] However, it was found that the SWNTs were fragmented, and most of the carbonaceous part ended up in the few-layer nanographene encapsulation of the fluoride NPs, whose growth was therefore limited to a great extent by the dual capping with the IL and nanographene layers. Although the exact cause of the graphitic encapsulation is unknown so far, surface defects (possibly stabilized by the capping of $Bmim^+$) may play a crucial role in this mechanism.

In contrast, the $C_{10}mim^+$ cation displays a stronger capability for self-assembly or supermolecular templating than smaller cations such as $Bmim^+$.[16] This likely leads to more extensive cation stacking over the first cation anchored on the SWNT surface, as in the columnar arrangement reported by Bellayer et al.[17] Hydrophilic BF_4^- anions and H_2O molecules are separated from these hydrophobic $C_{10}mim^+$ cations, with the possibility that $C_{10}mim^+$ cannot promptly cap the fluoride surface. In such a case, the surfaces of fluoride nuclei are exposed for further attachment of smaller particle units (i.e., crystal growth) until large octahedron-shaped crystals are formed. In this case of microphase separation, it was found that SWNT fragmentation did not occur, possibly because of the poor interaction between the defect-deficient surface of big grains and the IL layers capping the SWNTs.

From the viewpoint of mixed conductive networks,[3c] the fluoride-based microporous framework encapsulated by nanographene is expected to show better storage performance compared with unwired counterparts as well as the nonuniformly wired ones obtained using $C_{10}mimBF_4$. Figure 3a shows that the IL-sandwiched nanographene−$FeF_3{\cdot}0.5H_2O$ composite can be used as a 3 V Li storage cathode. The first discharge reached 143 mA h g^{-1} at 0.1C, corresponding to 0.63 Li insertion. The capacity was calculated on the basis of the total weight of fluoride and trapped IL. The plateaulike charge/discharge profiles did not substantially change in the following cycles, indicating the possible similarity of local environments of the defective pyrochlore and amorphized phases. The high symmetry between the charge and discharge profiles is ascribed to the facile ion diffusion in the interconnected 3D channels. A reversible capacity of ∼135 mA h g^{-1} was maintained during the following hundreds of cycles (Figure 3b). After 300 cycles, the discharge capacity of 114 mA h g^{-1} still corresponds to 0.5 Li insertion. Furthermore, the capacity was maintained at ∼80 mA h g^{-1} at 1C and could still be recovered to ∼140 mA h g^{-1} at 0.1C after cycling at the extremely high rate of 10C (Figure S7a). The excellent cyclability indicates good confinement of waters of hydration in the zigzag channels of the amorphized phase.

dx.doi.org/10.1021/ja402061q | J. Am. Chem. Soc. 2013, 135, 11425−11428

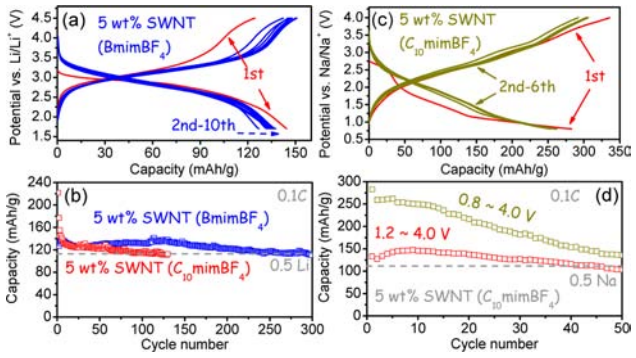

Figure 3. (a, c) Voltage vs capacity profiles of $FeF_3{\cdot}0.5H_2O$ cathodes wired by 5 wt % SWNTs at 0.1C during the first few cycles: (a) Li storage (from $BmimBF_4$) at 1.7−4.5 V and (c) Na storage (from $C_{10}mimBF_4$) at 0.8−4.0 V. (b, d) Discharge capacities of wired $FeF_3{\cdot}0.5H_2O$ at 0.1C and 25 °C as a function of cycle number for (b) Li storage at 1.7−4.5 V from $BmimBF_4$ (blue) and $C_{10}mimBF_4$ (red) and (d) Na storage from $C_{10}mimBF_4$ at 1.2−4.0 V (red) and 0.8−4.0 V (dark yellow). The theoretical reversible capacities for the 0.5 Li and 0.5 Na reactions are also labeled for comparison.

Interestingly, one should note that the electrodes consisting of big crystal grains (precipitated from $C_{10}mimBF_4$) resulted in much larger capacities (>220 mA h g^{-1}) for both Li and Na storage. We speculate that the higher capacity for big grains in the first few cycles may be associated with a slightly larger cavity size as well as less stuffing by capping IL. In the case of Li storage (Figures 3b and S8a), however, the following capacity gradually faded until it stabilized at 115 mA h g^{-1} after 100 cycles, indicating irreversible Li trapping in the channels. This phenomenon was significantly mitigated in the case of Na storage (Figure 3c), verifying its dependence on the cation size. The voltage for Na insertion was roughly 0.5 V lower than for Li insertion (Figure S8b). Staging-insertion behavior was observed during the first discharge, indicating Na-insertable sites of at least three different energies. During the following cycles, this phenomenon became less discernible, and instead sloped curves appeared along with slight improvements in both the reaction voltage and capacity. As a result of the open 3D channels, the voltage polarization was much smaller than in the dense ReO_3-type FeF_3 structure.[10] The alleviated Na trapping led to an extremely high reversible sodium capacity of ∼250 mA h g^{-1} at 0.1C over a voltage range of 0.8−4.0 V, corresponding to one electron transfer (Figure 3d). To the best of our knowledge, this is the highest Na storage capacity reported in a cathode voltage region, 2.5 times as large as that of ReO_3-type FeF_3.[10] A discharge capacity of 150 mA h g^{-1} was still preserved after 50 cycles. Better capacity retention would be expected upon further removal of the Na trapping phenomenon through channel decoration. Another approach to promote the rechargeability would be to intentionally decrease the amount of inserted Na by enhancing the low cutoff voltage to 1.2 V. A highly reversible average discharge capacity of 125 mA h g^{-1} was achieved within 50 cycles. The rate performance is comparable to that of Li storage because of the open structure (Figure S7b). It should be noted that capping/stuffing of the microporous framework would lower the Na diffusion kinetics and available insertable sites, as shown in the electrode consisting of IL-capping NPs (Figure S9), in view of the poor solubility of Na salts in ILs.[18]

In summary, we have reported a novel fluoride cathode having a pyrochlore-type open framework suited for Li as well as Na batteries. In a typical IL-based precipitation synthesis, the IL cations serve as structure-directing agents and remarkably influence the nucleation/growth behavior of the pyrochlore phase, leading to the generation of either defect-rich NPs (∼10 nm) encapsulated by few-layer nanographene or octahedron-shaped defect-deficient grains (200−300 nm) wired by SWNTs. The former are beneficial for achieving a long-life cathode with a reversible capacity of 135 mA h g^{-1} for Li batteries, while the latter enables a very high capacity of >220 mA h g^{-1} for both Li and Na batteries. These results motivate us to further explore open-structure prototypes characterized by intersecting tunnels and fluorinated frameworks, especially for next-generation post-lithium (e.g., Na and Mg) batteries.

■ ASSOCIATED CONTENT

Supporting Information

Procedures, additional data, and complete references. This material is available free of charge via the Internet at http://pubs.acs.org.

■ AUTHOR INFORMATION

Corresponding Author

chilinli@mail.sic.ac.cn

Notes

The authors declare no competing financial interest.

■ ACKNOWLEDGMENTS

The authors thank M. Konuma, G. Götz, B. Fenk, and Dr. R. Merkle for their technical help with XPS, XRD, SEM, and TGA−MS measurements. C.L. thanks the Hundred Talents Program of the Chinese Academy of Sciences for support.

■ REFERENCES

(1) (a) Férey, G.; et al. *Angew. Chem., Int. Ed.* **2007**, *46*, 3259. (b) Okubo, M.; et al. *J. Phys. Chem. Lett.* **2010**, *1*, 2063. (c) Ohkoshi, S.; et al. *J. Am. Chem. Soc.* **2010**, *132*, 6620. (d) Guloy, A. M.; et al. *Nature* **2006**, *443*, 320. (e) Cooper, E. R.; et al. *Nature* **2004**, *430*, 1012. (f) Hu, M.; et al. *J. Am. Chem. Soc.* **2012**, *134*, 2864.
(2) Recham, N.; et al. *Nat. Mater.* **2010**, *9*, 68.
(3) (a) Li, C. L.; et al. *Adv. Mater.* **2010**, *22*, 3650. (b) Li, C. L.; et al. *Adv. Funct. Mater.* **2011**, *21*, 1391. (c) Li, C. L.; et al. *ACS Nano* **2011**, *5*, 2930. (d) Li, C. L.; et al. *Chem. Mater.* **2013**, *25*, 962.
(4) (a) Slater, M. D.; et al. *Adv. Funct. Mater.* **2013**, *23*, 947. (b) Dunn, B.; et al. *Science* **2011**, *334*, 928.
(5) Shannon, R. D. *Acta Crystallogr.* **1976**, *A32*, 751.
(6) (a) Wessells, C. D.; et al. *Nano Lett.* **2011**, *11*, 5421. (b) Lu, Y. H.; et al. *Chem. Commun.* **2012**, *48*, 6544.
(7) (a) Sakao, M.; et al. *Solid State Ionics* **2012**, *225*, 502. (b) Cao, Y. L.; et al. *Adv. Mater.* **2011**, *23*, 3155. (c) Tepavcevic, S.; et al. *ACS Nano* **2012**, *6*, 530.
(8) (a) Ellis, B. L.; et al. *Nat. Mater.* **2007**, *6*, 749. (b) Shimizu, D.; et al. *Chem. Mater.* **2012**, *24*, 2598.
(9) (a) Arai, H.; et al. *J. Power Sources* **1997**, *68*, 716. (b) Badway, F.; et al. *J. Electrochem. Soc.* **2003**, *150*, A1209. (c) Li, H.; et al. *J. Electrochem. Soc.* **2004**, *151*, A1878. (d) Prakash, R.; et al. *J. Mater. Chem.* **2010**, *20*, 1871.
(10) Nishijima, M.; et al. *J. Power Sources* **2009**, *190*, 558.
(11) Fourquet, J. L.; et al. *Eur. J. Solid State Inorg. Chem.* **1988**, *25*, 535.
(12) Fukushima, T.; et al. *Science* **2003**, *300*, 2072.
(13) Li, C. L.; et al. *Adv. Energy Mater.* **2013**, *3*, 113.
(14) (a) Zhang, F. X.; et al. *Phys. Rev. Lett.* **2008**, *100*, No. 045503. (b) Crocombette, J. P.; et al. *Appl. Phys. Lett.* **2006**, *88*, No. 051912.
(15) Jacob, D. S.; et al. *Chem. Mater.* **2006**, *18*, 3162.
(16) Wang, T. W.; et al. *Langmuir* **2007**, *23*, 1489.
(17) Bellayer, S.; et al. *Adv. Funct. Mater.* **2005**, *15*, 910.
(18) Egashira, M.; et al. *Electrochim. Acta* **2011**, *58*, 95.